

**Accelerated-light-dark-matter–Earth inelastic scattering in direct detection**Liangliang Su<sup>1,\*</sup>, Lei Wu<sup>1,†</sup>, Ning Zhou<sup>2,‡</sup>, and Bin Zhu<sup>3,§</sup><sup>1</sup>*Department of Physics and Institute of Theoretical Physics, Nanjing Normal University, Nanjing, 210023, China*<sup>2</sup>*School of Physics and Astronomy, Shanghai Jiao Tong University, Key Laboratory for Particle Astrophysics and Cosmology (MOE) and**Shanghai Key Laboratory for Particle Physics and Cosmology, Shanghai 200240, China*<sup>3</sup>*School of Physics, Yantai University, Yantai 264005, China* (Received 14 December 2022; revised 1 May 2023; accepted 21 July 2023; published 1 August 2023)

The Earth-stopping effect plays a crucial role in the direct detection of sub-GeV dark matter. Besides the elastic scattering process, the quasielastic and deep inelastic scatterings between dark matter and nucleus that are usually neglected can dominate the interaction, especially in the accelerated dark matter scenarios, which may affect the dark matter detection sensitivity significantly for the underground experiments. We calculate such inelastic scattering contributions in the Earth-stopping effect and illustrate the essence of our argument with the atmospheric dark matter. With the available data, we find that the resulting upper limits on the atmospheric dark matter-nucleus scattering cross section can differ from those only considering the elastic scattering process by about 1 order of magnitude.

DOI: [10.1103/PhysRevD.108.035004](https://doi.org/10.1103/PhysRevD.108.035004)**I. INTRODUCTION**

There is overwhelming evidence for the existence of dark matter (DM), but the fundamental nature of DM remains a mystery. So far, many well-motivated DM candidates have been proposed, such as weakly interacting massive particles (WIMPs) [1,2], whose masses vary from  $\text{GeV}/c^2$  to  $\text{TeV}/c^2$ . However, there has been no conclusive evidence for WIMPs yet from underground experiments [3–5]. Beyond the WIMPs, the light DM with mass below  $\text{GeV}/c^2$  is another popular thermal candidate and is naturally predicted if the DM couples very weakly to the visible sector [6–12]. A large parameter space with the DM masses in the  $\text{keV}/c^2$  to  $\text{GeV}/c^2$  range is still unexplored by conventional direct detection experiments. It facilitates the development of new detection mechanisms and target materials (see the recent review, e.g., [13,14] and references therein).

Sub-GeV DM with large Lorentz boost is of particular interest, for instance, boosted DM [15–17], solar reflection

DM [18–21], cosmic ray boosted DM [22–34], and atmospheric DM (ADM) [35–39]. The kinetic energy of these accelerated DM particles can reach up to 1 GeV or even higher. This allows sub-GeV DM particles to induce detectable recoil signals in direct detection experiments. Note that, after being produced, the accelerated sub-GeV DM will pass through the Earth medium to reach underground detectors. Due to the DM-Earth interaction, they will lose energy and thus get attenuated, namely Earth-stopping effect [40–43]. In many previous works, only elastic scattering (ES) is considered in the DM-Earth interaction. This assumption is reasonable for DM with low kinetic energy. However, for accelerated DM, the quasielastic scattering (QES) and deep inelastic scattering (DIS), can dominate the DM-Earth interaction. The importance of this problem has been mentioned in [15,22,44,45]. Using the results of the neutrino-nucleus inelastic scattering in the standard model (SM), the impact was estimated in Ref. [45].

In this article we, for the first time, carry out the first principle calculation of the QES and DIS contributions in the Earth stopping effect for accelerated sub-GeV DM. We provide a general and consistent framework to obtain the sensitivity of the accelerated DM in direct detection. The sub-GeV ADM model with a scalar mediator is considered, where the collisions of cosmic rays with the atmosphere produce energetic mesons, and the mesons then decay into DMs. Such a DM particle obtains a large Lorentz boost from the decay of mesons. To model the DM propagation in the Earth, we take two benchmark models, “single

\*liangliangsu@njnu.edu.cn

†leiwu@njnu.edu.cn

‡nzhou@sjtu.edu.cn

§zhubin@mail.nankai.edu.cn

Published by the American Physical Society under the terms of the [Creative Commons Attribution 4.0 International license](https://creativecommons.org/licenses/by/4.0/). Further distribution of this work must maintain attribution to the author(s) and the published article’s title, journal citation, and DOI. Funded by SCOAP<sup>3</sup>.

scattering” [42] and “straight lines” [22,43]. Including the contributions of the inelastic scattering, we find the new upper bound of the ADM-nucleus scattering cross section can be changed by about 1 order of magnitude in comparison with that based on the elastic scattering only. Although we focus on the scalar mediator, our argument is general and can be extended to, for instance, vector mediator.

## II. DM-NUCLEUS INELASTIC SCATTERING

We calculate the DM-nucleus scattering in a simplified DM model with the scalar mediator [46]. The relevant DM-quark interactions are given by

$$\mathcal{L}_I = g_\chi S \bar{\chi}_L \chi_R + g_q S \bar{q}_L q_R, \quad (1)$$

where  $g_\chi$  and  $g_q$  are the couplings of mediator  $S$  with dark matter and quarks, respectively. We take  $q = \{u, \bar{u}\}$  in our calculations. The corresponding effective Lagrangian of DM-nucleus interaction can be written as [46,47]

$$\mathcal{L}_I = g_\chi S \bar{\chi}_L \chi_R + g_A S \bar{A}_L A_R F(Q^2), \quad (2)$$

where  $g_A = Zg_{pS} + (A - Z)g_{nS}$  are the couplings of mediator  $S$  with the nucleus  $A$ . The couplings  $g_{pS} = 0.014g_q m_p/m_q$  and  $g_{nS} = 0.012g_q m_n/m_q$  are the couplings of mediator  $S$  with proton and neutron, respectively. For simplicity, we assume  $g_{nS} = g_{pS}$  in our calculations. The nuclear form factor,  $F(Q^2)$ , takes the Helm form factor [48] in this work. As the inverse of momentum transfer to the scatterer is larger than the radius of the scatterer, the DM-nucleus scattering cross section is dominated by the elastic interaction, which is explicitly given in the Appendix. However, for a boosted sub-GeV DM, the QES and DIS processes must be considered in the high kinetic energy region. In the former, one or more nucleons are dislodged or excited inside atom  $A$ , but in the latter, the nucleus will disintegrate into a large number of hadrons.

### A. Deep inelastic scattering

Under the parton model, the DM-nucleus DIS can be simplified to  $\chi(k) + q(xp) \rightarrow \chi(k') + q'(p')$ , where  $x = Q^2/(2m_A\omega)$  is defined as the Bjorken scaling variable. It is a function of transfer energy  $\nu$  and the square of transfer momentum  $Q^2 \equiv -q^2 = -(k - k')^2 = 2E_\chi(E_\chi - \omega) - 2|\vec{k}||\vec{k}'|\cos\theta - 2m_\chi^2$ , where  $\theta$  is the scattering angle between DM and quarks. In the rest frame of the target particle, the differential cross section of DIS is given by

$$\frac{d\sigma_{\text{DIS}}}{d\omega dQ^2} = \sum_q \frac{\bar{\sigma}_n g_q^2 m_S^4 (4m_\chi^2 + Q^2)(4m_q^2 + Q^2) f_q^A(x, Q^2)}{32g_{pS}^2 \mu_n^2 m_A Q^2 (E_\chi^2 - m_\chi^2)(Q^2 + m_S^2)^2}, \quad (3)$$

where the momentum-independent DM-nucleon scattering cross section  $\bar{\sigma}_n \equiv g_\chi^2 g_{pS}^2 \mu_n^2 / \pi m_S^4$ . The function  $f_q^A(x, Q^2)$  is the nuclear parton distributions [49,50].

### B. Quasielastic scattering

At moderate incident energy, the DM elastically scatters with the quasifree nucleons bounded in a nucleus,  $\chi(k) + A(p_A) \rightarrow \chi(k') + X(\rightarrow N + Y)$ , which  $N$  and  $Y = (A - 1)$  denote nucleon and residual nucleus, respectively. In Born approximation, the double differential cross section of DM-nucleus QES via a scalar mediator can be given by

$$\frac{d\sigma_{\text{QE}}}{dE'_\chi d\Omega} = \frac{\bar{\sigma}_n m_S^4 |\vec{k}'|}{16\pi\mu_n^2 |\vec{k}|} \frac{\mathcal{X}^S W^S}{(Q^2 + m_S^2)^2}, \quad (4)$$

where  $E'_\chi$  is the outgoing DM energy. The DM tensor and nuclear tensor,  $\mathcal{X}^S$  and  $W^S$ , are defined as

$$\begin{aligned} \mathcal{X}^S &= \sum \langle \chi | j_\chi^S | \chi' \rangle \langle \chi' | j_\chi^S | \chi \rangle = 4m_\chi^2 + Q^2; \\ W^S &= \sum \langle A | J^S(0) | X \rangle \langle X | J^S(0) | A \rangle \delta(p_i - p_f), \end{aligned} \quad (5)$$

where  $j_\chi^S$  and  $J^S$  are the DM and nuclear scalar current operators, respectively. In the low momentum transfers,  $W^S$  can be obtained by the nuclear many-body theory [51] which regards the initial and final states as nonrelativistic wave functions, and the current operator is expanded by the Taylor series of  $|\vec{q}|/m_N$ . However, the nonrelativistic wave functions are improper for the final state  $|X\rangle$  with high momentum transfer, for instance, the incident energy of DM is larger than several hundred MeV.

The IA is an excellent scheme to calculate the inclusive cross section of QES for the high momentum transfer [52–56]. It assumes that i) the DM-nucleus scattering is reduced to the incoherent sum of the scattering processes involving individual nucleons; ii) the nucleon  $N$  and residual nucleus  $(A - 1)$  after scattering are independent. We neglect the dynamical final state interactions but consider the effect of Pauli blocking in this work. Under the IA scheme, the nuclear current operator  $J^S(0)$  can be calculated as the sum of individual nucleon currents  $J^S \rightarrow \sum_N j_N^S$ , and the final state  $|X\rangle$  can be separated to the knockout nucleon  $|x, \vec{p}'\rangle$  and the residual nucleus  $|Y, \vec{p}_Y\rangle$ , as shown in Fig. 1,  $|X\rangle \rightarrow |x, \vec{p}'\rangle \otimes |Y, \vec{p}_Y\rangle$ .

The inclusive differential cross section of the DM-nucleus QES can be given by

$$\frac{d\sigma_{\text{QE}}}{dE'_\chi d\Omega} = Z \frac{d\sigma_p}{dE'_\chi d\Omega} + (A - Z) \frac{d\sigma_n}{dE'_\chi d\Omega}, \quad (6)$$

with

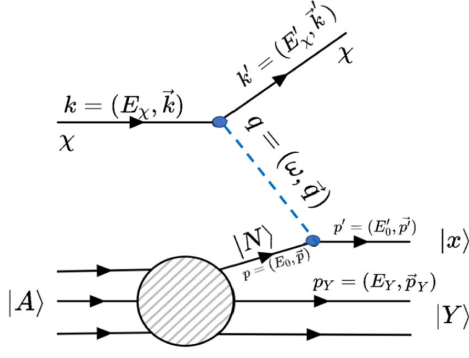


FIG. 1. The diagrammatic sketch of DM-nucleus QES under the impulse approximation (IA) scheme.

$$\frac{d\sigma_N}{dE'_\chi d\Omega} = \frac{\bar{\sigma}_n m_S^4}{16\pi\mu_n^2(Q^2 + m_S^2)^2} \frac{|\vec{k}'|}{|\vec{k}|} \int d^3\vec{p} dE \frac{m_N^2}{E_{\vec{p}} E_{\vec{p}'}} P(\vec{p}, E) \times \Theta(|\vec{p}'| - p_F) \delta(\omega - E + m_N - E'_0) \mathcal{X}^S H_N^S. \quad (7)$$

Here  $N = \{p, n\}$  and  $\Theta(|\vec{p}'| - p_F)$  come from the nuclear Pauli blocking, and  $p_F$  is Fermi momentum. Note that  $m_N/E_{\vec{p}}$  and  $m_N/E_{\vec{p}'}$  are the covariant normalization factors. The hadronic tensor,  $H^S$ , is defined by

$$H_N^S = \sum \langle N, \vec{p} | j_N^S | x, \vec{p} + \vec{q} \rangle \langle \vec{p} + \vec{q}, x | j_N^S | N, \vec{p} \rangle = \frac{1}{2} \text{Tr} \left[ \Gamma^S \frac{\not{p} + m_N}{2m_N} \Gamma^{S\dagger} \frac{\not{p}' + m_N}{2m_N} \right], \quad (8)$$

with

$$\Gamma^S = F_S(Q^2), \quad (9)$$

where  $F_S(Q^2)$  is the scalar nucleon form factor [57]. In this work, we employ the scalar form factor  $F_S(Q^2)/F_S(0)$  in

Ref. [58], where the scalar form factor at  $Q^2 = 0$  has already been incorporated into the nucleon coupling  $g_{pS}$ . It should be noted that the transfer momentum  $Q$  in Eq. (7) is not only transferred to the interacting nucleon but also the residual nucleus system. Thus, we have to handle the problem with the off-shell kinematics [59], i.e.,  $q \equiv (\omega, \vec{q}) \rightarrow \tilde{q} \equiv (\tilde{\omega}, \vec{q})$ , where the transfer energy  $\tilde{\omega} = E_{\vec{p}'} - E_{\vec{p}} = \omega - E + m_N - E_{\vec{p}}$ . The spectral function of the target nucleus,  $P(\vec{p}, E)$  in Eq. (7), represents the probability of removing a nucleon with momentum  $\vec{p}$  and removal energy  $E$  from the bound state of the nucleus [52,60],

$$P(\vec{p}, E) = \sum_Y |\langle A | Y, \vec{p}_Y \rangle \langle N, \vec{p} \rangle|^2 \delta(E - m_N + E_0 - E_Y). \quad (10)$$

In Fig. 2, we show the ratio of scattering cross sections,  $R_{\sigma_i} \equiv \sigma_i/\sigma_{\text{tot}}$ , as the function of the DM kinetic energy  $T_\chi$  for different mediator masses, where  $i = \text{ES, QES, DIS}$ . We consider the oxygen and iron nuclei in the Earth, which are the most abundant elements in bulk Earth, and their number density profiles can be obtained from Ref. [61,62]. It can be seen that the contribution of each process depends on the scalar mediator mass. For instance, when  $m_S = 0.03$  GeV, the cross section of the elastic scattering (blue lines) is always larger than the inelastic scattering (red and green lines). However, for  $m_S = 0.3$  GeV/ $c^2$ , the QES becomes the dominant contribution in  $T_\chi \gtrsim 200$  MeV range. If  $m_S = 30$  GeV/ $c^2$ , then the DIS is non-negligible when  $T_\chi \gtrsim 1$  GeV. These results can be understood as follows: the elastic and inelastic scattering processes occur in the low and high momentum transfer  $Q$  regions, respectively. When the mediator mass  $m_S$  is much smaller than the typical value of  $Q_{\text{ES}}$ , the elastic scattering cross section can be enhanced by  $\sim 1/Q_{\text{ES}}^4$  as compared with the

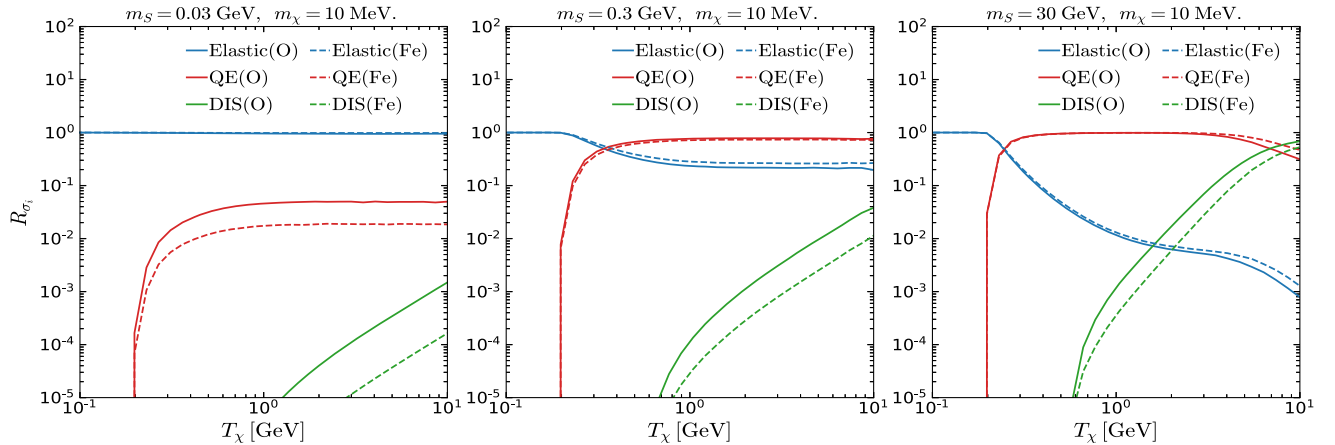


FIG. 2. The ratio  $R_{\sigma_i}$  as the function of DM kinetic energy  $T_\chi$  at the DM mass  $m_\chi = 10$  MeV for different mediator masses  $m_S = 0.03$  GeV (left panel),  $0.3$  GeV (middle panel), and  $30$  GeV (right panel). The solid and dotted lines denote the DM-oxygen and DM-iron scattering, respectively.

inelastic scattering processes, due to  $Q_{\text{ES}} \ll Q_{\text{QES,DIS}}$ . On the other hand, if the mediator mass  $m_S$  is much larger than  $Q_{\text{ES}}$ , then this enhancement in elastic scattering disappears. Such behaviors also appear in the DM-nucleus scattering via exchanging a dark photon, where the QES and DIS are dominant when the dark photon mass is greater than  $\mathcal{O}(1)$  GeV. These findings were missed in Ref. [45] because it is based on the assumption of the heavy  $Z$  mediator and  $V - A$  interaction. For a general case, e.g., a light mediator or other interactions, their approach is not applicable.

### III. EARTH STOPPING

We take the ADM as a boosted DM benchmark model and consider the contribution of the proton ( $p$ ) in cosmic rays (CRs) colliding with the nitrogen ( $N$ ) in the atmosphere. ADM is produced by the inelastic collision between the CRs and the atmosphere on Earth, i.e.,  $p + N \rightarrow M \rightarrow \chi\bar{\chi} + X$ , where the meson  $M$  promptly decays into the DM pair  $\chi\bar{\chi}$  and other SM particles  $X$  via an on-shell scalar mediator  $S$ . We focus on  $\eta$  meson decay process,  $\eta \rightarrow \pi^0 S(\rightarrow \chi\bar{\chi})$ , which requires the mediator mass  $m_S$  to satisfy  $2m_\chi < m_S < m_\eta - m_{\pi^0}$ . Besides, given the constraints from the MINIBoONE experiment and the kaon meson decays [63,64], we adopt the appropriate parameters,  $m_S = 300 \text{ MeV}/c^2$  and  $\text{Br}[\eta \rightarrow \pi S(\rightarrow \chi\bar{\chi})] = 10^{-5}$ .

Then, we use two benchmark Earth-stopping models to show the effects of inelastic scattering on the flux of the ADM reaching the detector. One model assumes that the ADM scatters with nuclei at most once, i.e., the ‘‘single scatter’’ approximation [42]. Thus, the differential flux of the ADM around the detector is given by

$$\frac{d\Phi_\chi^z}{dT_\chi^z} = 2\pi \int_{-1}^1 \mathcal{P}_{\text{surv}}(T_\chi, \cos \theta) \frac{d\Phi_\chi}{dT_\chi d\Omega} d\cos \theta, \quad (11)$$

where  $T_\chi^z$  is the kinetic energy of the ADM at the detector.  $\mathcal{P}_{\text{surv}}$  is the survival probability of the ADM as it reaches the detector. The explicit calculation is given in the Appendix.

The other model assumes that the DM particles travel in straight lines and lose energy due to the DM-Earth scattering, which we refer to as straight lines approximation [43]. The ADM differential flux around the detector is given by

$$\frac{d\Phi_\chi^z}{dT_\chi^z} = \int \frac{dT_\chi}{dT_\chi^z} \frac{d\Phi_\chi}{dT_\chi d\Omega} d\Omega. \quad (12)$$

Here  $dT_\chi/dT_\chi^z$  can be obtained by solving the energy loss function [22,45]. Although there are some Monte Carlo simulations of DM trajectories [65–71], these two benchmark models are enough to show the effects of inelastic scattering in the Earth-stopping.

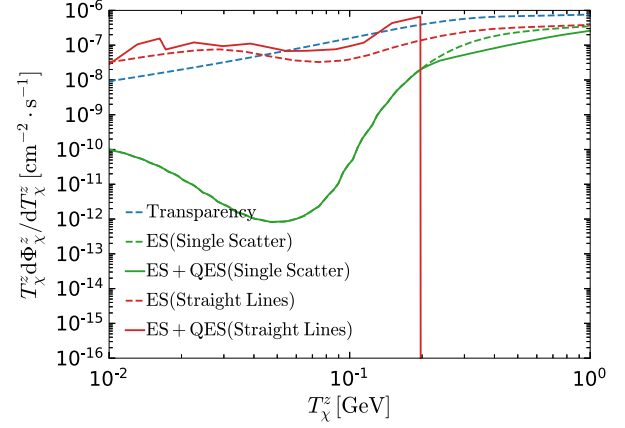


FIG. 3. The expected differential flux of ADM at the Xenon1T experiment for single scatter (green lines) and straight lines (red lines) without (dotted lines) and with (solid lines) QES. Here we assume  $m_\chi = 0.01 \text{ GeV}/c^2$ ,  $m_S = 300 \text{ MeV}/c^2$ ,  $\bar{\sigma}_n = 5 \times 10^{-29} \text{ cm}^2$ , and  $\text{Br}[\eta \rightarrow \pi S(\rightarrow \chi\bar{\chi})] = 10^{-5}$ . The result in the transparent Earth case is also plotted (blue dotted line).

Figure 3 shows the expected differential flux of ADM reaching the Xenon1T detector. Since the number of DIS events is negligible in the ADM (see Fig. 2), we consider the contribution of the QES, which becomes sizable in the DM kinetic energy region,  $T_\chi \gtrsim 200 \text{ MeV}$ . Including the QES can enhance the DM-Earth scattering cross section, and thus reduce the ADM flux at the detector in the high  $T_\chi$  region. In the straight lines approximation, ADMs travel along straight lines and lose energy as they interact with nuclei. This makes a portion of highly boosted ADMs that involve in the QES contribute to the low energy region as comparison with the transparent Earth and single scatter cases. For example, a  $\sim 10 \text{ MeV}$  ADM with an initial energy of  $T_\chi \sim 1 \text{ GeV}$  could be shifted to  $T_\chi^z \sim 0.1 \text{ GeV}$  region. On the other hand, ADMs for the single scatter approximation undergo, at most, one scattering as they travel through the Earth. The differential ADM flux at the detector is almost negatively correlated with the scattering cross section [cf. Eqs. (11) and (A2)]. Therefore, the ADM flux for the single scatter approximation is greatly reduced in  $T_\chi \in [0.01, 0.1] \text{ GeV}$  because the DM-nucleus ES cross section is enhanced by the momentum transfer effect of the light DM [72]. While for the larger  $T_\chi$ , the ES cross section is highly suppressed by the nuclear form factor.

### IV. EXCLUSION LIMITS

With the above differential flux, we can evaluate the nuclear recoil rate of the ADM in Xenon1T experiment,

$$R = N_T \int_{E_R^{\min}}^{E_R^{\max}} dE_R \int_{T_\chi^{\min}}^{T_\chi^{\max}} \epsilon(E_R) \frac{d\Phi_\chi^z}{dT_\chi^z} \frac{d\sigma}{dE_R} dT_\chi^z, \quad (13)$$

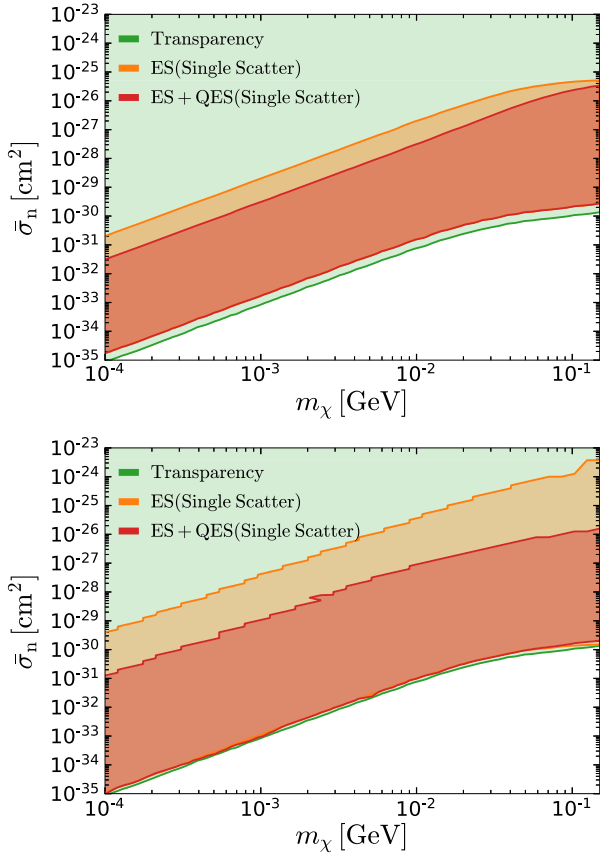


FIG. 4. The exclusion limits on the momentum-independent ADM-nucleon scattering cross section  $\bar{\sigma}_n \equiv g_\chi^2 g_{pS}^2 \mu_n^2 / \pi m_S^4$  versus the DM mass  $m_\chi$  for single scatter (upper panel) and straight lines (lower panel). The green, orange, and red regions denote the results for the transparent Earth, Earth stopping with the ES only, and with ES plus QES, respectively. We assume  $m_S = 300$  MeV and  $\text{Br}[\eta \rightarrow \pi S(\rightarrow \chi\bar{\chi})] = 10^{-5}$ .

where  $N_T$  and  $\epsilon$  are the number density of Xenon and the detector efficiency with the nuclear recoil energy  $E_R$ , respectively. Based on the 90% confidence level data of Xenon1T [73], we employ the method in Ref. [22] to derive the exclusion limits. In Fig. 4, we show the exclusion limits on the momentum-independent ADM-nucleon scattering cross section  $\bar{\sigma}_n$ . We can see that there are upper bounds on scattering cross section  $\bar{\sigma}_n$  because of the Earth-stopping effect. Besides, comparing with the ES only, we find that the upper bounds including the DM-Earth QES can be changed by about 1 order of magnitude. Note that the upper limits in the “straight line” approximation are likely overestimated because the scattering of our sub-GeV DM against heavy nuclei in the reality would yield a recoil angle that is roughly isotropic in the frame of the Earth. On the other hand, the lower bounds are almost the same even considering QES because the Earth-stopping effect is very weak for the small scattering cross section. However,

in the single scatter approximation, there is a factor of 2 difference between the lower bounds for (quasi-)elastic scattering and transparency. This arises from the fact that the DMs are likely scattered away during their traveling from the hemisphere behind the detector. Consequently, for single scatter, almost half of the DMs are unable to reach the detector as a comparison with the transparency approximation. In contrast, for the straight lines approximation, all DMs traveling toward the detector will reach it, albeit with some energy loss in their traveling. The amount of energy loss is determined by the DM-nucleus scattering cross section. For the lower limits, due to the very small scattering cross section, DMs can still produce observable nuclear recoil energy. Thus, the lower bounds in straight lines approximation are similar to those in the transparency approximation.

## V. CONCLUSION

Based on the first principle calculations, we find that the inelastic accelerated sub-GeV DM-Earth scattering can be the dominant contribution in the Earth-stopping effect. The mediator mass will affect the relative size of the elastic and inelastic scattering cross sections. Including the inelastic contribution in the Earth-stopping effect can change the upper bound on the DM-nucleus scattering by about 1 order of magnitude in the Xenon1T direct detection.

## ACKNOWLEDGMENTS

We are grateful to Artur M. Ankowski for the helpful discussions. This work is supported by the National Natural Science Foundation of China (NNSFC) under Grants No. 12275134, No. 12275232, and No. 11835005.

## APPENDIX

### 1. Coherent DM-nucleus elastic scattering

The differential cross section of coherent DM-nucleus elastic scattering is given by

$$\frac{d\sigma_{\text{ES}}}{dE_R} = \frac{\bar{\sigma}_n A^2 m_S^4 F^2(E_R)}{32 \mu_n^2 m_A (2m_A E_R + m_S^2)^2 (E_\chi^2 - m_\chi^2)} \times (4m_\chi^2 + 2m_A E_R)(4m_A^2 + 2m_A E_R), \quad (\text{A1})$$

where  $E_\chi$  is the incoming DM energy, and  $\mu_n$  is the reduced mass of DM and nucleon. The recoil energy  $E_R = Q^2/2m_A$  is the function of momentum transfer  $Q$  and nucleus mass  $m_A$ .

### 2. Survival probability

The survival probability in single scatter approximation is defined as

$$\mathcal{P}_{\text{surv}}(T_\chi, \cos \theta) = \exp\left(-\sum_i \frac{d_{\text{eff},i}(\cos \theta)}{\bar{\lambda}_i(T_\chi)}\right). \quad (\text{A2})$$

Here  $\theta$  is the angle between DM incoming direction and the Earth's core/detector axis. Note that  $\bar{\lambda}_i = [\sigma_i^{\text{tot}}(T_\chi)\bar{n}_i]^{-1}$  is the average mean free path, and  $n_i(\bar{n}_i)$  is the (average) number density of Earth species  $i$ . The effective Earth-crossing distance,  $d_{\text{eff},i}(\cos \theta)$ , is defined by

$$d_{\text{eff},i} \approx \begin{cases} \int_{R_E \sin \theta}^{R_E} \frac{2rn_i(r)dr}{\bar{n}_i \sqrt{r^2 - R_E^2 \sin^2 \theta}}; & \theta \in \left[0, \frac{\pi}{2}\right] \\ \int_{R_E - z_D}^{R_E} \frac{n_i(r)}{\bar{n}_i} dr, & \theta \in \left[\frac{\pi}{2}, \pi\right], \end{cases} \quad (\text{A3})$$

where  $R_E = 6378.14$  km and  $z_D = 1.4$  km are the Earth's radius and the depth of Xenon1T experiment, respectively.

- 
- [1] B. W. Lee and S. Weinberg, *Phys. Rev. Lett.* **39**, 165 (1977).  
[2] G. Jungman, M. Kamionkowski, and K. Griest, *Phys. Rep.* **267**, 195 (1996).  
[3] E. Aprile *et al.* (XENON Collaboration), *Phys. Rev. Lett.* **123**, 251801 (2019).  
[4] Q. Wang *et al.* (PandaX-II Collaboration), *Chin. Phys. C* **44**, 125001 (2020).  
[5] J. Aalbers *et al.* (LZ Collaboration), arXiv:2207.03764.  
[6] R. Essig, J. Mardon, and T. Volansky, *Phys. Rev. D* **85**, 076007 (2012).  
[7] R. Essig, T. Volansky, and T.-T. Yu, *Phys. Rev. D* **96**, 043017 (2017).  
[8] K. Schutz and K. M. Zurek, *Phys. Rev. Lett.* **117**, 121302 (2016).  
[9] S. Knapen, T. Lin, and K. M. Zurek, *Phys. Rev. D* **96**, 115021 (2017).  
[10] R. T. D'Agnolo, C. Mondino, J. T. Ruderman, and P.-J. Wang, *J. High Energy Phys.* **08** (2018) 079.  
[11] G. Bertone and T. M. P. Tait, *Nature (London)* **562**, 51 (2018).  
[12] G. Elor, R. McGehee, and A. Pierce, *Phys. Rev. Lett.* **130**, 031803 (2023).  
[13] M. Battaglieri *et al.*, U.S. cosmic visions: New ideas in dark matter, arXiv:1707.04591.  
[14] Y. Kahn and T. Lin, *Rep. Prog. Phys.* **85**, 066901 (2022).  
[15] K. Agashe, Y. Cui, L. Necib, and J. Thaler, *J. Cosmol. Astropart. Phys.* **10** (2014) 062.  
[16] J. Berger, Y. Cui, and Y. Zhao, *J. Cosmol. Astropart. Phys.* **02** (2015) 005.  
[17] K. Agashe, Y. Cui, L. Necib, and J. Thaler, *J. Phys. Conf. Ser.* **718**, 042041 (2016).  
[18] H. An, M. Pospelov, J. Pradler, and A. Ritz, *Phys. Rev. Lett.* **120**, 141801 (2018); **121**, 259903(E) (2018).  
[19] T. Emken, *Phys. Rev. D* **105**, 063020 (2022).  
[20] H. An, H. Nie, M. Pospelov, J. Pradler, and A. Ritz, *Phys. Rev. D* **104**, 103026 (2021).  
[21] C. V. Cappiello, N. P. A. Kozar, and A. C. Vincent, *Phys. Rev. D* **107**, 035003 (2023).  
[22] T. Bringmann and M. Pospelov, *Phys. Rev. Lett.* **122**, 171801 (2019).  
[23] Y. Ema, F. Sala, and R. Sato, *Phys. Rev. Lett.* **122**, 181802 (2019).  
[24] C. V. Cappiello and J. F. Beacom, *Phys. Rev. D* **100**, 103011 (2019); **104**, 069901(E) (2021).  
[25] W. Wang, L. Wu, J. M. Yang, H. Zhou, and B. Zhu, *J. High Energy Phys.* **12** (2020) 072; **02** (2021) 52(E).  
[26] S.-F. Ge, J. Liu, Q. Yuan, and N. Zhou, *Phys. Rev. Lett.* **126**, 091804 (2021).  
[27] G. Guo, Y.-L. S. Tsai, M.-R. Wu, and Q. Yuan, *Phys. Rev. D* **102**, 103004 (2020).  
[28] C. Xia, Y.-H. Xu, and Y.-F. Zhou, *Nucl. Phys.* **B969**, 115470 (2021).  
[29] Y. Ema, F. Sala, and R. Sato, *SciPost Phys.* **10**, 072 (2021).  
[30] N. F. Bell, J. B. Dent, B. Dutta, S. Ghosh, J. Kumar, J. L. Newstead, and I. M. Shoemaker, *Phys. Rev. D* **104**, 076020 (2021).  
[31] J.-C. Feng, X.-W. Kang, C.-T. Lu, Y.-L. S. Tsai, and F.-S. Zhang, *J. High Energy Phys.* **04** (2022) 080.  
[32] W. Wang, L. Wu, W.-N. Yang, and B. Zhu, *Phys. Rev. D* **107**, 073002 (2023).  
[33] X. Cui *et al.* (PandaX-II Collaboration), *Phys. Rev. Lett.* **128**, 171801 (2022).  
[34] T. N. Maity and R. Laha, arXiv:2210.01815.  
[35] J. Alvey, M. Campos, M. Fairbairn, and T. You, *Phys. Rev. Lett.* **123**, 261802 (2019).  
[36] L. Su, W. Wang, L. Wu, J. M. Yang, and B. Zhu, *Phys. Rev. D* **102**, 115028 (2020).  
[37] C. A. Argüelles, V. Muñoz, I. M. Shoemaker, and V. Takhistov, *Phys. Lett. B* **833**, 137363 (2022).  
[38] L. Darmé, *Phys. Rev. D* **106**, 055015 (2022).  
[39] M. Du, R. Fang, and Z. Liu, arXiv:2211.11469.  
[40] C. Kouvaris and I. M. Shoemaker, *Phys. Rev. D* **90**, 095011 (2014).  
[41] R. Foot and S. Vagnozzi, *Phys. Lett. B* **748**, 61 (2015).  
[42] B. J. Kavanagh, R. Catena, and C. Kouvaris, *J. Cosmol. Astropart. Phys.* **01** (2017) 012.  
[43] B. J. Kavanagh, *Phys. Rev. D* **97**, 123013 (2018).  
[44] P. deNiverville, C.-Y. Chen, M. Pospelov, and A. Ritz, *Phys. Rev. D* **95**, 035006 (2017).  
[45] J. Alvey, T. Bringmann, and H. Kolesova, *J. High Energy Phys.* **01** (2023) 123.  
[46] B. Batell, A. Freitas, A. Ismail, and D. Mckeen, *Phys. Rev. D* **100**, 095020 (2019).  
[47] D. Aristizabal Sierra, V. De Romeri, and N. Rojas, *Phys. Rev. D* **98**, 075018 (2018).  
[48] G. Duda, A. Kemper, and P. Gondolo, *J. Cosmol. Astropart. Phys.* **04** (2007) 012.

- [49] A. Buckley, J. Ferrando, S. Lloyd, K. Nordström, B. Page, M. Rüfenacht, M. Schönherr, and G. Watt, *Eur. Phys. J. C* **75**, 132 (2015).
- [50] R. Abdul Khalek, R. Gauld, T. Giani, E. R. Nocera, T. R. Rabemananjara, and J. Rojo, *Eur. Phys. J. C* **82**, 507 (2022).
- [51] J. Carlson and R. Schiavilla, *Rev. Mod. Phys.* **70**, 743 (1998).
- [52] O. Benhar, N. Farina, H. Nakamura, M. Sakuda, and R. Seki, *Phys. Rev. D* **72**, 053005 (2005).
- [53] A. M. Ankowski and J. T. Sobczyk, *Phys. Rev. C* **74**, 054316 (2006).
- [54] A. M. Ankowski and J. T. Sobczyk, *Phys. Rev. C* **77**, 044311 (2008).
- [55] A. M. Ankowski, O. Benhar, T. Mori, R. Yamaguchi, and M. Sakuda, *Phys. Rev. Lett.* **108**, 052505 (2012).
- [56] A. M. Ankowski and O. Benhar, *Phys. Rev. D* **88**, 093004 (2013).
- [57] G. Eichmann, Hadron matrix elements, <http://cftp.ist.utl.pt/~gernot.eichmann/2020-QCDHP/QCD-hadron-matrix-elements.pdf>.
- [58] R. C. Schardmüller, Master's thesis, Graz U., 2013.
- [59] T. De Forest, *Nucl. Phys.* **A392**, 232 (1983).
- [60] O. Benhar, A. Fabrocini, S. Fantoni, and I. Sick, *Nucl. Phys.* **A579**, 493 (1994).
- [61] W. McDonough, in *Treatise on Geochemistry*, edited by H. D. Holland and K. K. Turekian (Pergamon, Oxford, 2003), pp. 547–568, ISBN: 978-0-08-043751-4.
- [62] J. Lundberg and J. Edsjo, *Phys. Rev. D* **69**, 123505 (2004).
- [63] A. A. Aguilar-Arevalo *et al.* (MiniBooNE DM Collaboration), *Phys. Rev. D* **98**, 112004 (2018).
- [64] A. V. Artamonov *et al.* (BNL-E949 Collaboration), *Phys. Rev. D* **79**, 092004 (2009).
- [65] T. Emken and C. Kouvaris, *J. Cosmol. Astropart. Phys.* **10** (2017) 031.
- [66] T. Emken and C. Kouvaris, *Phys. Rev. D* **97**, 115047 (2018).
- [67] M. S. Mahdawi and G. R. Farrar, *J. Cosmol. Astropart. Phys.* **10** (2018) 007.
- [68] T. Emken, Ph.D. thesis, Southern Denmark U., CP3-Origins, 2019.
- [69] Y. Chen, B. Fornal, P. Sandick, J. Shu, X. Xue, Y. Zhao, and J. Zong, *Phys. Rev. D* **107**, 033006 (2023).
- [70] C. Xia, Y.-H. Xu, and Y.-F. Zhou, *J. Cosmol. Astropart. Phys.* **02** (2022) 028.
- [71] Z. Z. Liu *et al.* (CDEX Collaboration), *Phys. Rev. D* **105**, 052005 (2022).
- [72] V. V. Flambaum, L. Su, L. Wu, and B. Zhu, *Sci. China Phys. Mech. Astron.* **66**, 271011 (2023).
- [73] E. Aprile *et al.* (XENON Collaboration), *Phys. Rev. Lett.* **121**, 111302 (2018).